JACS
JOURNAL OF THE AMERICAN CHEMICAL SOCIETY

Communication

pubs.acs.org/JACS

Synthesis of Structurally Ordered Pt_3Ti and Pt_3V Nanoparticles as Methanol Oxidation Catalysts

Zhiming Cui,[†] Hao Chen,[†] Mengtian Zhao, Daniel Marshall, Yingchao Yu, Héctor Abruña, and Francis J DiSalvo*

Department of Chemistry and Chemical Biology, Baker Laboratory, Cornell University, Ithaca, New York 14853-1301, United States

Supporting Information

ABSTRACT: Structurally ordered Pt_3Ti or Pt_3V intermetallic nanoparticle catalysts with ultrasmall particle sizes have never been successfully synthesized. Herein, we present a KCl-nanoparticle method to successfully provide such compounds. These two catalysts show enhanced catalytic activity and stability for methanol oxidation compared to pure Pt.

Direct methanol fuel cells (DMFCs) are of potential interest for portable energy needs, since liquid methanol has a high volumetric energy compared to compressed hydrogen gas.[1−3] Pt transition-metal alloys have been widely used as the catalysts due to their tunable electronic structure.[4−6] However, due to the disordered nature of alloy, these bimetallic catalysts still suffer poisoning behavior as their Pt counterparts.[2,4,7] Nevertheless, structurally ordered intermetallic phases of such alloy systems, on the other hand, provide much better control over electronic structure and, more importantly, the local geometry of metal atoms. Not only does the activity increase, but also the poisoning effect is largely alleviated.[8,9] As an example, intermetallic PtPb nanoparticles show mass-specific activities toward formic acid oxidation about 10 times higher than commercial PtRu.[10] PtBi intermetallic phase exhibits superior performance in formic acid oxidation compared to Pt (higher current density and lower onset potentials).[11] The discovery of Pt-based ordered intermetallic catalysts containing late 3d transition metals leads us to explore Pt-based intermetallic compounds containing early 3d transition metals.

However, it is extremely difficult to synthesize clean Pt-3d transition-metal intermetallic nanoparticles with small particle sizes. First, the early 3d transition metals are extremely oxyphilic and much less electronegative compared to the late 3d transition metals. To reduce their appropriate precursors and incorporate them into Pt lattice requires an ultrafast and powerful reducing process, which ultimately means using a strong reducing agent such as organoborohydrides or Na naphthalide.[14,15,17] To achieve an ordered structure, a thermal annealing process at elevated temperatures of 600 °C and beyond is necessary. Furthermore, the synthesis of metallic nanoparticles often relies on the use of organic surfactant molecules to stabilize particles against agglomeration. This approach may be successful for late 3d transition metals. However, such methods can not provide the required reduction kinetics and often decompose, producing carbonacious surface deposits, during the thermal anealing processes. As a result, control of the particle size with a surfactant free method still remains a great challenge. Previously we successfully tuned the synthetic process and achieved structually ordered Pt-transition-metal nanocompounds with all the desired properties.[12] However, the process was limited to the late 3d transition metals.

Here we successfully prepared the 6 nm structurally ordered Pt_3Ti and Pt_3V nanoparticles using a surfactant-free nanoparticle-KCl matrix method in air-free conditions and an aprotic solvent (THF). Potassium triethylborohydride (KEt_3BH) was used as the reducing agent due to its fast reduction kenetics. As reported in our earlier work, the byproduct KCl serves as the matrix for the co-produced Pt_3M particles.[12,13] The nanoparticle growth occurs only slowly by a particle-particle coalescense mechanism during annealing.[13] The density of Pt-M nanoparticles in the KCl matrix and the annealing conditions are the two main factors controling the resultant particle sizes. The preparation procedure is shown schematically in Figure S1. The following reactions illustrate the formation of Pt-based nanopaticles in THF using the above method:

$$3PtCl_4 + TiCl_4 + 64LiCl + 80KEt_3BH = Pt_3Ti + 80KCl + 8H_2 + 16Et_3B + 64LiEt_3BH \quad (1)$$

$$3PtCl_4 + VCl_3 + 65LiCl + 80KEt_3BH = Pt_3V + 80KCl + 7.5H_2 + 15Et_3B + 15Et_3B + 65LiEt_3BH \quad (2)$$

$$3PtCl_4 + 68LiCl + 80KEt_3BH = 3Pt + 80KCl + 6H_2 + 12Et_3B + 68LiEt_3BH \quad (3)$$

Pt_3M nanoparticles are immediately formed after the addition of reducing agent, KEt_3BH. Meanwhile the byproduct, KCl, is simultaneously generated. KCl is insoluble in THF[14] and serves as an encapsulant which prevents the agglomeration of the Pt-M nanoparticles. During thermal annealing, the KCl matrix greatly reduces the coalescence of nanoparticles, which consequently controls the particle growth process and ultimately the particle sizes.[13] One of the issues of using hydride as reducing agent is the potential formation of metal hydrides, which may impede with the formation of homoge-

Received: May 7, 2014
Published: July 7, 2014

   dx.doi.org/10.1021/ja504573a | J. Am. Chem. Soc. 2014, 136, 10206−10209

neous alloy or ordered intermetallic phases. This becomes a significant concern when reducing early 3d transition metals, owing to their stable hydride phases. Assuming the hydrides do form during reduction, the enthalpy of formation of these hydrides as well as Pt-M alloys can be used to calculate the transition temperature between the hydride and the alloy. As the temperature increases, the reaction to form intermetallic phases becomes spontaneous. During the thermal annealing process, the following equations can be used to describe such transitions.

$$TiH_2(s) + 3Pt(s) \leftrightarrow Pt_3Ti(s) + H_2(g) \quad (4a)$$

$$VH_2(s) + 3Pt(s) \leftrightarrow Pt_3V(s) + H_2(g) \quad (4b)$$

At a certain temperature, if ΔG becomes negative, the equilibrium will move toward the alloying product direction and the PtM alloy will be formed releasing H_2 gas. The temperatures where the free energy favors the alloying reaction of Pt and Ti (or V) are 467 K for Pt_3Ti and 352 K for Pt_3V. The detailed calculated results are shown in Table S1. In our experiments, to obtain the structurally ordered intermetallic phases of Pt_3M (M = Ti and V), the samples were annealed at 650−700 °C, which is much higher than these transition temperatures. Finally, ethylene glycol is used to dissolve the KCl and transiently stabilize Pt_3M nanoparticles until they bind to the catalyst support. The detailed process is shown in the Supporting Information.

Figures 1 and S2 show the pXRD patterns for Pt/C, Pt_3Ti/C, and Pt_3V/C. As expected for an FCC structure with a = 3.9230

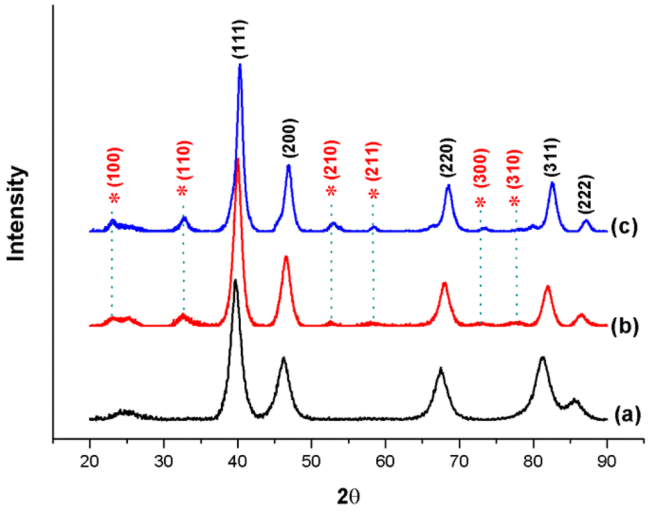

Figure 1. XRD patterns of Pt/C (a), Pt_3Ti/C (b), and Pt_3V/C (c). The peaks that appear due to ordering of the Pt and M are marked with a *.

(1) Å, the pXRD pattern for Pt/C shows five peaks at 39.7°, 46.2°, 67.5°, 81.3°, and 85.7°. After annealing, the nanoparticles in Pt_3Ti/C and Pt_3V/C crystallized in a cubic space group *Pm*-3*m* with refined lattice parameters a = 3.8970(1) Å and 3.8870(1) Å, respectively. Compared to Pt/C, six additional peaks with Miller indices 100, 110, 210, 211, 300, and 310 are apparent. They correspond to the ordering reflections of Pt_3M (Ti and V) in the Cu_3Au structure type.[9] Compared to Pt/C, the pXRD peaks of Pt_3M (Ti and V) slightly shift to higher angles due to their smaller lattice constant relative to Pt. The average domain sizes for Pt/C, Pt_3Ti/C and Pt_3V/C, are 5.5, 6.5, and 6.2 nm, respectively, as calculated by the Debye−Scherrer equation.

TEM images of Pt/C, Pt_3Ti/C, and Pt_3V/C and their corresponding particle diameter histograms are presented in Figure S3. Histograms of metal nanoparticle diameters for more than 100 randomly chosen particles were obtained. The average metal particles sizes in the Pt/C, Pt_3Ti/C, and Pt_3V/C catalysts as estimated from their histograms are 5.3 ± 0.4, 6.1 ± 0.5, and 5.8 ± 0.6 nm, respectively. The size of as-prepared ordered Pt_3Ti particles using this method is much smaller than that obtained previously (~37 nm).[9] The particle sizes of these catalysts determined by TEM are slightly smaller than the domain size determined from the XRD peaks, indicating that the nanoparticles are mainly single crystals.[15] To better visualize the ordered intermetallic structure, we have also studied the atomic level arrangement of Pt and Ti (or V) by high-resolution TEM (HR-TEM). In Figure 2a,c, Pt_3Ti and

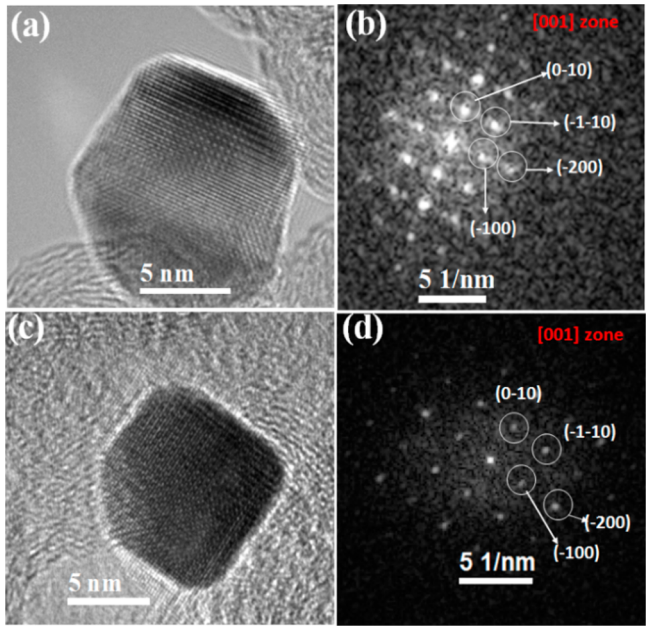

Figure 2. HR-TEM images of Pt_3Ti/C (a) and its corresponding FFT image of the atomic arrangement (b); HR-TEM images of Pt_3V/C (c) and its corresponding FFT image of the atomic arrangement (d).

Pt_3V nanoparticles are oriented along the [001] zone axis. Since the unique super periods are present only in the structurally ordered intermetallic phase and are absent in the disordered alloy phase, the ordered intermetallic structure can be directly visualized. For example, along the [001] axis of the ordered intermetallic structure, the projected unit cell comprises a periodic square array of Ti (or V) followed by Pt columns at the edges and corners of each unit cell. Such ordered arrangements can be directly obtained from the diffraction patterns from the fast Fourier transform (FFT) patterns, as shown in Figure 2b,d. For example, the intermetallic structure of Pt_3Ti can be identified with the presence of superlattice reflection signals in the electron diffraction pattern of a single crystal domain. As shown in Figure 2b, the spacings of the {100} and {110} superlattice spots are observed as 3.897 and 2.756 Å, respectively, which match with the bulk Pt_3Ti intermetallic structure. The diffraction patterns also align with the simulated intermetallic phase (Figure S4a). In the case of Pt_3V, the superlattice spacings at {100} and {110} appear at

dx.doi.org/10.1021/ja504573a | J. Am. Chem. Soc. 2014, 136, 10206−10209

3.887 and 2.749 Å, as expected for ordered Pt_3V. The diffraction patterns match with the simulated Pt_3V intermetallic phase (Figure S4b).

The actual metal loadings in Pt_3Ti/C, Pt_3V/C, and Pt/C are 28.4, 28.6, and 32.3 wt %, respectively, which were analyzed by thermogravimetric analysis (TGA) from 40 to 550 °C under air, as shown in Figure S5. The atomic ratios of Pt/M in Pt_3M (Ti and V) were determined by energy-dispersive X-ray spectroscopy (EDS), as shown in Figure S6, to be 3.08 ± 0.2 for Pt_3Ti/C and 2.91 ± 0.3 for Pt_3V/C. These results are consistent with the ratios of Pt/M (Ti and V) in the reactant mixture (with a Pt-to-M mole ratio of 3). STEM-EDS mapping of Pt_3Ti/C and STEM-EDS line spectra of Pt_3V/C are shown in Figure S7. Both suggest that the Pt and Ti/V are uniformly distributed in the nanoparticles.

Figure 3a shows typical linear sweep voltammograms performed in 0.1 M HClO4 + 1 M CH_3OH at a scan rate of

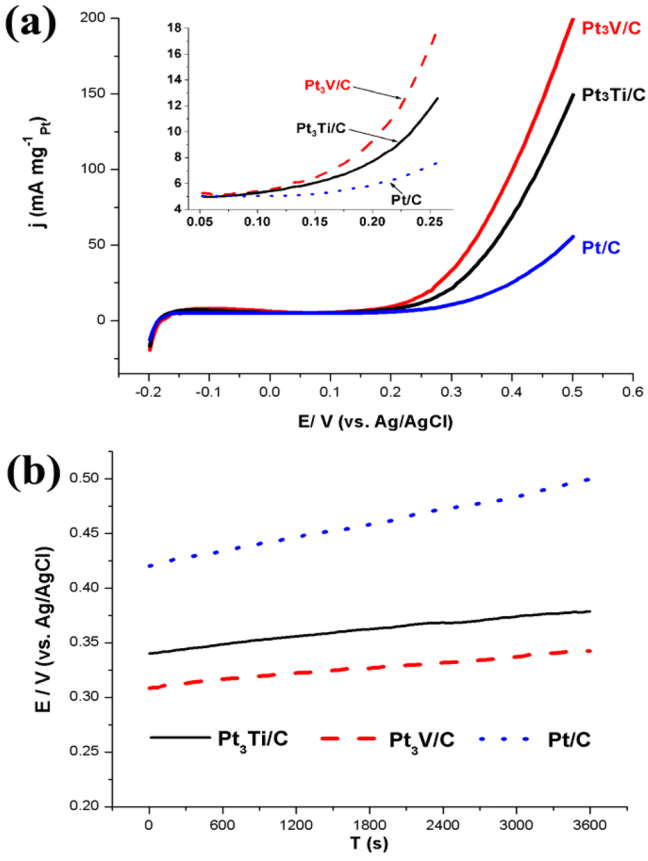

Figure 3. (a) Linear sweep voltammograms performed in 0.1 M $HClO_4$ + 1 M CH_3OH at a scan rate of 20 mV s^{-1}. The inset shows the partial magnification of linear sweep voltammograms; (b) potential vs time plots measured by chronopotentiometry at a constant load of 1 mA cm^{-2} in 0.1 M $HClO_4$ + 1 M CH_3OH.

20 mV s^{-1}. The results of all samples tested are presented in Table 1. When these three catalysts are compared for their relative activity, two significant parameters are the onset potentials and the oxidation current at a given potential.[16] Thermodynamically, the equilibrium potential of methanol electro-oxidation is about −0.15 V (vs Ag/AgCl).[1,4] Good catalysts should produce oxidation currents at relatively low overpotentials. As shown in the inset of Figure 3a, the onset potential on Pt_3Ti/C and Pt_3V/C is 0.07 V, which is 100 mV

Table 1. ECSA, Onset Potentials, Mass Activities, and Specific Activities for Pt_3Ti, Pt_3V, and Pt/C Catalysts

			mass activities (mA mg^{-1}_{Pt})		specific activities (A m^{-2}_{Pt})	
samples	ECSA (m^2 g^{-1})	onset potentials (vs Ag/AgCl)	0.3 V	0.5 V	0.3 V	0.5 V
Pt_3Ti/C	48.7	0.07 V	23.7	149.4	0.049	0.307
Pt_3V/C	52.1	0.07 V	35.7	200.2	0.069	0.384
Pt/C	58.8	0.17 V	10.4	53.6	0.017	0.091

more negative than that on Pt/C. It is also more negative than the reported values (0.14−0.2 V) on PtRu/C catalysts.[3,9] While there is some variation in current density between Pt_3Ti and Pt_3V intermetallic samples, they both show much better activities than Pt/C catalyst. For example, at a given potential of o.5 V, the current densities for Pt_3Ti/C and Pt_3V/C are 149.4 and 200.2 mA mg^{-1}_{Pt}, which are ∼3 and ∼4 times higher than those for Pt/C at the corresponding potentials. These three catalysts examined have different particle size and composition. To further investigate the role of composition, the specific surface activities of these three catalysts are also evaluated. The specific surface activities of these catalysts could be obtained by normalizing currents with electrochemically active specific surface area (ECSA), which is determined by CO_{ad} stripping method.[17,18] The CO_{ad} stripping voltammograms for these three catalysts are presented in Figure S8. Note that the hydrogen desorption peaks in the low potential region are absent, since the surface is saturated by CO_{ad}. The CO_{ad} species are oxidized and removed from the catalyst surface at potentials above 0.4 V. The ECSAs calculated from the CO_{ad} oxidation charge after subtracting the background current are also presented in Table 1. The two carbon supported Pt_3M intermetallic catalysts exhibit much higher surface activities than Pt/C catalyst. For example, the specific surface activities at 0.5 V for the Pt_3Ti/C and Pt_3V/C catalysts are 0.307 and 0.384 mA cm^{-2}_{Pt}. In sharp contrast, Pt/C just produces specific surface activities of 0.091 mA cm^{-2}_{Pt} at 0.5 V. In addition, as shown in Figure S8, the onset potentials of CO_{ad} oxidation on Pt_3Ti/C and Pt_3V/C are 0.40 and 0.42 V, respectively, which are over 60 mV more negative than that on Pt/C (0.52 V), indicating that the addition of second metal (V and Ti) facilitates the removal of CO and diminishes the poisoning of the catalysts. The enhanced activity of the Pt_3M catalyst when compared with Pt for methanol oxidation might be attributed to a bifunctional mechanism.[19] The cyclic voltammograms of the catalysts from −0.2 to 1 V are shown in Figure S9. These three catalysts display similar electrochemical behavior during methanol oxidation. In the forward scans, the peaks at ∼0.7 V for the three catalysts are typical for methanol oxidation. The oxidation peaks at ∼0.5 V in the reverse scan are known to be due to residual carbon species formed in the forward scan. We conclude that methanol is not completely oxidized in the forward scan for these catalysts, since there is a large peak in the reverse scan. On the other hand, the peak current densities for Pt_3Ti/C (380 mA·mg^{-1}_{Pt}) and Pt_3V/C (481 mA·mg^{-1}_{Pt}) are much higher than for Pt/C (161 mA·mg^{-1}_{Pt}), suggesting that Pt_3Ti/C and Pt_3V/C have higher activities for methanol oxidation.

The stability of the catalysts is assessed by chronopotentiometry at a constant current of 1 mA·cm^{-2} as shown in Figure 3b. The onset potentials on Pt_3Ti/C (0.34 V) and Pt_3V/C (0.31 V) are more negative than that of Pt/C (0.42 V), which

dx.doi.org/10.1021/ja504573a | J. Am. Chem. Soc. 2014, 136, 10206−10209

indicates that these two ordered Pt_3M catalysts have higher catalytic activity relative to Pt/C. The potential change due to surface poisoning or changes in morphology in 1 h are 34, 41, and 80 $mV{\cdot}h^{-1}$ for Pt_3V/C, Pt_3Ti/C, and Pt/C, respectively. Apparently, two Pt_3M intermetallic catalysts exhibit lower voltage degradation rates than Pt/C, indicating that Pt_3M catalysts are more durable than Pt/C. The durability of these three catalysts is also determined by chronoamperometry curves which are shown in Figure S10. When the potential is fixed at 0.6 V, all catalysts show an initial rapid current decay, likely attributed to the formation of surface oxidation species, such as CO_{ads} and CHO_{ads}.[20] However, the stable mass specific currents for methanol oxidation reaction on Pt_3V/C and Pt_3Ti/C catalysts are ~46 and ~39 mA mg^{-1}_{Pt}, which are significantly higher than Pt/C (~17 mA mg^{-1}_{Pt}). The stability of these catalysts is further studied using linear sweep voltammograms by applying potential between −0.2 and 0.5 V in electrolytes of 0.1 M HClO4 + 1 M CH_3OH. Plots of currents at 0.5 V versus cycle numbers are shown in Figure S11. After 1000 cycles, the current densities at 0.5 V are reduced by 27.2% for Pt_3Ti/C and 23.4% for Pt_3V/C, which are significantly less than that for Pt/C (40.7%), demonstrating that ordered Pt_3Ti/C and Pt_3V/C catalysts have better catalytic stability. As shown in Figure S12, ordered Pt_3Ti/C and Pt_3V/C catalysts exhibit enhanced catalytic activity and stability relative to their corresponding alloys.

In conclusion, structurally ordered Pt_3Ti and Pt_3V with ultrasmall particle sizes were synthesized under air-free conditions with THF as solvent and with KEt_3BH as the reducing agent. KCl is an insoluble byproduct which encases the nanoparticles, preventing agglomeration. During the thermal annealing process, the KCl matrix controls the particle size by greatly slowing particle coalescence. Pt_3Ti and Pt_3V nanoparticles are crystalline and structurally ordered, as confirmed by XRD and HR-TEM. For methanol oxidation, one typical anode reaction, ordered Pt_3Ti/C and Pt_3V/C exhibit significant enhancement in activity and durability compared to Pt. This synthesis strategy to prepare structurally ordered intermetallic should be generally applicable to a wide variety of ordered binary and ternary phases.

■ ASSOCIATED CONTENT

Ⓢ Supporting Information

Synthesis of Pt_3M/C (Ti and V) and Pt/C; electrode preparation and electrochemical measurements; XRD patterns, TGA, and EDX of samples; electrochemical results for samples. This material is available free of charge via the Internet at http://pubs.acs.org/.

■ AUTHOR INFORMATION

Corresponding Author

fjd3@cornell.edu

Author Contributions

†These authors contributed equally.

Notes

The authors declare no competing financial interest.

■ ACKNOWLEDGMENTS

This work was supported by the Energy Materials Center at Cornell, an Energy Frontier Research Center funded by the U.S. Department of Energy, Office of Basic Energy Sciences under award no. DE-SC0001086.

■ REFERENCES

(1) Aricò, A. S.; Srinivasan, S.; Antonucci, V. *Fuel Cells* **2001**, *1*, 133.
(2) Arico, A. S.; Bruce, P.; Scrosati, B.; Tarascon, J. M.; Van Schalkwijk, W. *Nat. Mater.* **2005**, *4*, 366.
(3) Cui, Z.; Liu, C.; Liao, J.; Xing, W. *Electrochim. Acta* **2008**, *53*, 7807.
(4) Demirci, U. B. *J. Power Sources* **2007**, *173*, 11.
(5) Hammer, B.; Nørskov, J. K. *Surf. Sci.* **1995**, *343*, 211.
(6) Greeley, J.; Nørskov, J. K. *Surf. Sci.* **2005**, *592*, 104.
(7) Roth, C.; Benker, N.; Buhrmester, T.; Mazurek, M.; Loster, M.; Fuess, H.; Koningsberger, D. C.; Ramaker, D. E. *J. Am. Chem. Soc.* **2005**, *127*, 14607.
(8) Casado-Rivera, E.; Volpe, D. J.; Alden, L.; Lind, C.; Downie, C.; Vázquez-Alvarez, T.; Angelo, A. C. D.; DiSalvo, F. J.; Abruña, H. D. *J. Am. Chem. Soc.* **2004**, *126*, 4043.
(9) Abe, H.; Matsumoto, F.; Alden, L. R.; Warren, S. C.; Abruña, H. D.; DiSalvo, F. *J. Am. Chem. Soc.* **2008**, *130*, 5452.
(10) Alden, L. R.; Han, D. K.; Matsumoto, F.; Abruna, H. D.; DiSalvo, F. J. *Chem. Mater.* **2006**, *18*, 5591.
(11) Casado-Rivera, E.; Gal, Z.; Angelo, A. C. D.; Lind, C.; DiSalvo, F. J.; Abruna, H. D. *ChemPhysChem* **2003**, *4*, 193.
(12) Chen, H.; Wang, D.; Yu, Y.; Newton, K. A.; Muller, D. A.; Abruña, H.; DiSalvo, F. J. *J. Am. Chem. Soc.* **2012**, *134*, 18453.
(13) Chen, H.; Yu, Y.; Xin, H. L.; Newton, K. A.; Holtz, M. E.; Wang, D.; Muller, D. A.; Abruña, H. D.; DiSalvo, F. J. *Chem. Mater.* **2013**, *25*, 1436.
(14) Strong, J.; Tuttle, T. R. *J. Phys. Chem.* **1973**, *77*, 533.
(15) Warren, B. X-ray Diffraction; Dover Publications: Mineola, NY, 1990.
(16) Ghosh, T.; Leonard, B. M.; Zhou, Q.; DiSalvo, F. J. *Chem. Mater.* **2010**, *22*, 2190.
(17) Takasu, Y.; Fujiwara, T.; Murakami, Y.; Sasaki, K.; Oguri, M.; Asaki, T.; Sugimoto, W. *J. Electrochem. Soc.* **2000**, *147*, 4421.
(18) Kawaguchi, T.; Sugimoto, W.; Murakami, Y.; Takasu, Y. *Electrochem. Commun.* **2004**, *6*, 480.
(19) Watanabe, M.; Motoo, S. *J. Electroanal. Chem. Interfacial Electrochem.* **1975**, *60*, 275.
(20) Kabbabi, A.; Faure, R.; Durand, R.; Beden, B.; Hahn, F.; Leger, J. M.; Lamy, C. *J. Electroanal. Chem.* **1998**, *444*, 41.